C.P. No. 213
(16,779)
A.R.C. Technical Report

C.P. No. 213
(16,779)
A.R.C. Technical Report

MINISTRY OF SUPPLY

AERONAUTICAL RESEARCH COUNCIL

CURRENT PAPERS

Pressure Distributions: Axially Symmetric Bodies in Oblique Flow

By

I. J. Campbell and R. G. Lewis

LONDON HER MAJESTY'S STATIONERY OFFICE

1955

THREE SHILLINGS NET

C.P. No.213

ADMIRALTY RESEARCH LABORATORY, TEDDINGTON, MIDDLESEX

A.R.L./R.I/G/HY/19/1

PRESSURE DISTRIBUTIONS: AXIALLY SYMMETRIC BODIES IN OBLIQUE FLOW

by

I. J. Campbell and R.G. Lewis

ABSTRACT

A simple picture, known from the work of I. Lotz, of the flow over the forward part of a body of revolution in oblique flow is derived here from entirely elementary considerations. The pressure at any point of the (forward part of the) body at any angle of incidence depends on three parameters whose values vary along the body. The variation of these parameters along the body can be determined from a relatively small number of wind tunnel or water tunnel measurements. The necessary water tunnel measurements have been made for four axially symmetric head shapes. Additional measurements have been made to illustrate the theoretical conclusions. The data for each head shape are adequate for a determination of the pressure coefficient at any point on the head shapes at any angle of incidence (up to 6°, say). In particular they can be used to determine the peak suction at any angle of incidence and so the conditions for the onset of cavitation on the head.

INTRODUCTION

1. Some measurements of the pressure distribution along various axially symmetric bodies, held at an angle of incidence to the stream have been made in the A.R.L. 12-inch water tunnel. A simple picture of the flow, which was known previously from the fairly elaborate theoretical development of I. Lotz (Ref. 1), is derived here from entirely elementary considerations. It will be seen that the pressure at any point on the forward part of the body, when held at any angle of incidence, can be deduced from a relatively small number of measurements: the measurements, reported here, are used to illustrate this. The results will find application in the prediction of the conditions for the onset of nose cavitation at various angles of incidence.

THEORETICAL CONSIDERATIONS

2.1 The following considerations, concerning the oblique flow past a body of revolution, are based on the assumption of potential flow. The assumption will, generally speaking, be legitimate over the forward part of the body where the boundary layer is thin. It will not apply near the downstream end of the body. Nor will it apply very near the tip of a body with a point at its upstream end.

2.2 Consider the potential flow past a body of revolution when the axis is inclined at an angle α to the stream (Fig. 1). At any point on the surface of the body the velocity may be divided into the following components:

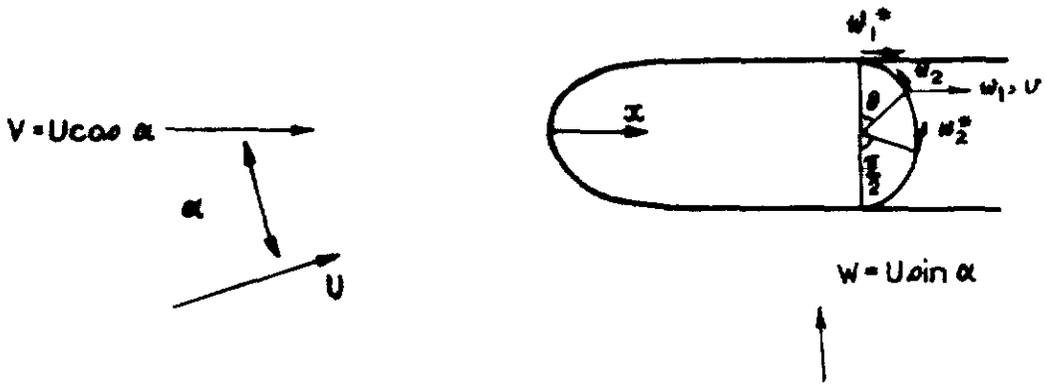

FIGURE 1

v, directed along the meridian and associated with the longitudinal component, V, of the stream velocity.

w_1, also directed along the meridian and associated with the transverse component, W, of the stream velocity.

The particular value of w_1, when the azimuthal angle θ is 0°, is denoted by w_1^*.

w_2, directed perpendicular to the meridian and also associated with W. The particular value of w_2, when $\theta = \pi/2$, is denoted by w_2^*.

v, w_1 and w_2 are functions of x, the axial distance from the nose, and in addition w_1 and w_2 depend also on θ.

2.3 Clearly at any point

$$\frac{v}{V} = (1 - C_{p_o})^{\frac{1}{2}}, \qquad (1)$$

where C_{p_o} is the pressure coefficient measured at that point in purely axial flow. (The pressure coefficient is defined in para. 2.7.)

2.4 It will now be shown that w_1 depends on θ in an extremely simple way. Consider the velocity induced along the meridian at a particular station, x, by a purely transverse flow. In Fig. 2(a) the free stream velocity is of

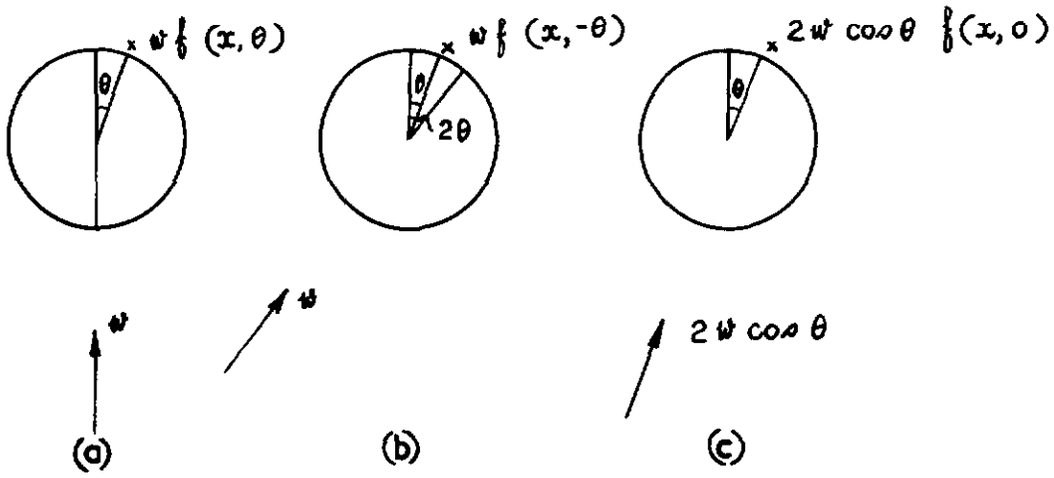

FIGURE 2

magnitude ω and is parallel to the meridian plane of zero azimuthal angle: the velocity component along the meridian at station x and azimuthal angle θ is proportional to ω and otherwise depends only on x and on the angle between the meridian plane containing the position on the surface of the body and the meridian plane to which the free stream velocity is parallel; this velocity component will therefore be written $\omega f(x,\theta)$. In Fig. 2 (b) the free stream velocity is of magnitude ω and is parallel to the meridian plane of azimuthal angle 2θ: the velocity component at station x and azimuthal angle θ is $\omega f(x,-\theta)$ and is clearly equal to $\omega f(x,\theta)$. In Fig. 2 (c) the free stream velocity is of magnitude $2\omega \cos\theta$ and is parallel to the meridian plane of azimuthal angle θ: the velocity component along the meridian at station x and azimuthal angle θ is $2\omega \cos\theta f(x,o)$. Since the flow of Fig. 2 (c) is simply the flow obtained by compounding the flows of Fig. 2 (a) and Fig. 2 (b) in the manner appropriate to potential flows, it follows that

$$f(x,\theta) = f(x,o) \cos\theta.$$

This implies, in the notation of Fig. 1, that

$$w_1 = w_1^* \cos\theta \qquad (2)$$

2.5 The dependence of w_2 on θ can be derived in a similar way. In Fig. 3 (a) the free stream velocity is of magnitude ω and is parallel to the meridian

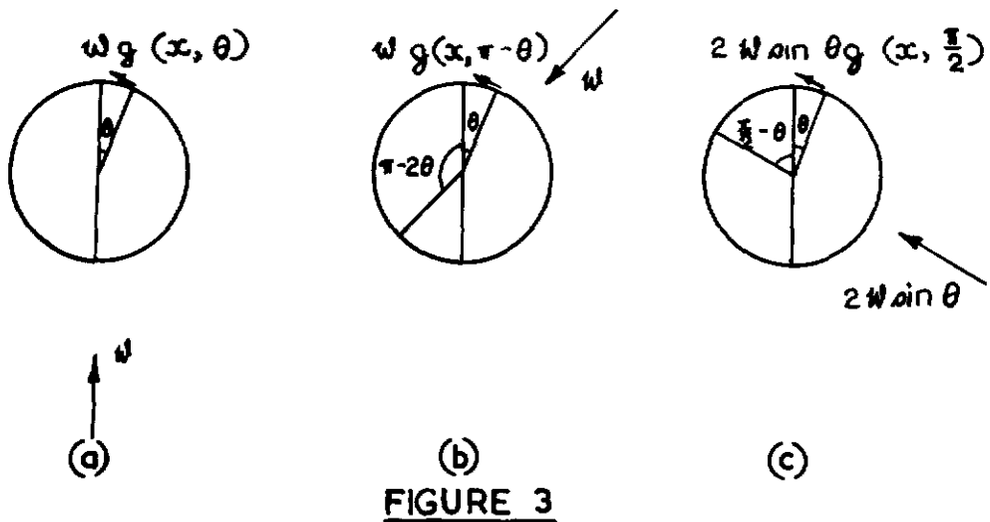

FIGURE 3

plane of zero azimuthal angle: the velocity component perpendicular to the meridian at station x and azimuthal angle θ will be written $\omega g(x,\theta)$. In Fig. 3 (b) the free stream velocity is of magnitude ω and is parallel to the meridian plane of azimuthal angle $-(\pi-2\theta)$: the velocity perpendicular to the meridian at station x and azimuthal angle θ is $\omega g(x,\pi-\theta)$ and is seen to equal $\omega g(x,\theta)$ by reversing the flow. In Fig. 3 (c) the free stream velocity is of magnitude $2\omega \sin\theta$ and is parallel to the meridian plane of azimuthal angle $-\left(\frac{\pi}{2} - \theta\right)$: the velocity component perpendicular to the meridian at station x and azimuthal angle θ is $2\omega \sin\theta g\left(x,\frac{\pi}{2}\right)$. Since the flow of Fig. 3 (c) is the flow obtained by compounding the flows of Fig. 3(a) and Fig. 3(b), it follows that

$$g(x,\theta) = g\left(x,\frac{\pi}{2}\right)\sin\theta.$$

This implies, in the notation of Fig. 1, that

$$w_2 = w_2^* \sin\theta \tag{3}$$

2.6 These results, that w_1 is proportional to $\cos\theta$ and that w_2 is proportional to $\sin\theta$, *can be found in Ref. 1, where they emerge after a great* deal of elaborate analysis. The proof given here offers the advantage of simplicity and the results emerge directly as a consequence of the compounding properties of potential flows.

2.7 For the flow of Fig. 1 it follows from Bernoulli's theorem that

$$p_s + \tfrac{1}{2}\rho U^2 = p + \tfrac{1}{2}\rho\left\{(v + w_1)^2 + w_2^2\right\},$$

where p_s is the free stream pressure and p is the pressure at any point on the surface of the body;

i.e.
$$C_p \equiv \frac{p - p_s}{\frac{1}{2}\rho U^2} = 1 - \frac{(v + w_1)^2}{U^2} - \frac{w_2^2}{U^2}$$

$$= 1 - \left(\frac{v}{V}\right)^2\left(\frac{V}{U}\right)^2 - 2\left(\frac{v}{V}\right)\left(\frac{w_1}{W}\right)\left(\frac{V}{U}\right)\left(\frac{W}{U}\right) - \left(\frac{w_1}{W}\right)^2\left(\frac{W}{U}\right)^2 - \left(\frac{w_2}{W}\right)^2\left(\frac{W}{U}\right)^2$$

$$= 1 - (1-C_{p_o})\cos^2\alpha - \left(\frac{w_1}{W}\right)^*(1-C_{p_o})^{\frac{1}{2}}\cos\theta \sin 2\alpha -$$

$$\left(\frac{w_1}{W}\right)^{*2}\cos^2\theta \sin^2\alpha - \left(\frac{w_2}{W}\right)^{*2}\sin^2\theta \sin^2\alpha$$

$$\therefore C_p - C_{p_o} = (1 - C_{p_o})(1 - \cos^2\alpha) - \frac{w_1}{W}^*(1 - C_{p_o})^{\frac{1}{2}}\cos\theta \sin 2\alpha - \left(\frac{w_1}{W}\right)^{*2}\cos^2\theta$$

$$\sin^2\alpha - \left(\frac{w_2}{W}\right)^{*2}\sin^2\theta \sin^2\alpha \tag{4}$$

2.8 Thus, when the parameters, C_{p_o}, $\frac{w_1}{W}^*$ and $\frac{w_2}{W}^*$, are known, the pressure coefficient at any position on the nose at any angle of incidence can be calculated. C_{p_o} can be found by a measurement of pressures along any meridian at zero angle of incidence. Knowing C_{p_o}, $\frac{w_1}{W}^*$ can be found by a measurement of pressures along the meridian, $\theta = 0$, with the model inclined at a non-zero angle of pitch. Likewise $\frac{w_2}{W}^*$ can be found by a measurement of pressures along the meridian, $\theta = \frac{\pi}{2}$, with the model inclined at a non-zero angle of pitch. From C_{p_o}, $\frac{w_1}{W}^*$ and $\frac{w_2}{W}^*$, it would also be possible to determine the streamlines on the surface of an axially symmetric body at any angle of incidence.

EXPERIMENTAL ARRANGEMENT

3.1 The pressure measurements were made on a 2-inch diameter model in the A.R.L. 12-inch water tunnel in the fixed wall working section.† The model and support arrangements are shown diagrammatically in Fig. 4.

3.2 The model is made up of an interchangeable nose-piece, a number of tubular sections spigoted together, a centre section carried on a support strut and a tail fairing. A long $\frac{5}{8}$-inch diameter bolt, extending from the nose-piece to the centre section, clamps the various sections together.

3.3 Seventeen pressure points are arranged on the surface of the model, holes of $\frac{1}{52}$-inch diameter being drilled through from outside and terminating on the inner walls in short lengths of copper tubing. These are connected to the front bulkhead of the centre section by P.V.C. tubing, which allows sufficient flexibility to enable the forward part of the model, which carries the pressure points, to rotate about the model axis. Adjustment in the azimuthal position of the holes is made from section AA. By undoing the through bolt sufficiently to slide the peg out of its locating slot in the spigot, the whole front portion and nose-piece together can be turned through 180°: locating slots are provided at 15° intervals. Access to the bolt is obtained by removing the top cover of the working section and unscrewing the tail fairing.

3.4 The centre section of the model is rigidly fixed to a single stainless steel strut, hollow and of streamline section. This strut terminates in a 1-inch o.d. circular tube which passes through the gland: by sliding this tube up and down, the model can be located vertically from outside the tunnel. Down the strut and tube pass seventeen copper tubes, which transmit the pressure readings, picking up with the appropriate P.V.C. tubes on the front bulkhead of the centre section. Two typical pressure measuring lines, one from the nose and one from the cylindrical portion of the model, are shown in Fig. 4.

3.5 The angle of pitch can be adjusted from outside the tunnel. This is effected by the pivot pin and spherical gland arrangement shown in the sketch. Since the model rotates about the pivot pin, an adjustment in pitch calls for an adjustment in vertical position also. A pair of slots cut into the strut tube register with tongues fixed to the frame supporting the pitching arrangements: in this way the model is held at zero yaw.

TUNNEL CORRECTIONS

4.1 Since the measurements were made in a fixed wall jet, it was necessary to apply corrections for tunnel pressure gradient and for blockage.

4.2 A point on the tunnel axis 16 inches downstream of the throat pressure tapping was used as reference point. The water speed and static pressure at the reference point were determined in a preliminary calibration in terms of the pressure drop across the contraction and the throat pressure. The point on the axis of the model at the forward end of the cylindrical portion was maintained at the reference point as closely as possible in all measurements. A correction was added to all pressure measurements on the model according to the distance of the measuring point from the reference point and the pressure gradient obtaining in the empty tunnel: this correction never exceeded $\frac{1}{2}\%$ of the velocity head. The same correction was applied at a given pressure hole at all angles of incidence: this is justifiable since the static pressure distribution over the centre of the working section is flat within the order of accuracy of the present measurements (about 1% of the velocity head) and the axial shift of any hole due to changes of incidence never exceeded $\frac{1}{10}$ inch (to which the corresponding change in pressure due to the tunnel pressure gradient is $\frac{1}{100}\%$ of the velocity head).

4.3 If U denotes the tunnel velocity,

v_h the velocity at any point on the model (as determined by the measured pressure),

† The tunnel has interchangeable working section of different types.

$v_h - \Delta v_h$ the velocity at the same point on the model, corrected for blockage,

p_s the free stream static pressure (allowance for the tunnel pressure gradient being made separately as already discussed),

p_m the pressure measured at the point of interest on the model,

and p_c the pressure at the same point on the model, corrected for blockage,

then, since the total head is unaltered by blockage,

$$p_m + \tfrac{1}{2}\rho v_h^2 = p_s + \tfrac{1}{2}\rho U^2 = p_c + \tfrac{1}{2}\rho(v_h - \Delta v_h)^2$$

It follows that the blockage correction is given approximately by

$$\Delta C_p \equiv \frac{p_c - p_m}{\tfrac{1}{2}\rho U^2} = 2(1 - C_p)\frac{\Delta v_h}{U} \qquad (5)$$

The velocity induced by blockage at any point on the surface of the model was assumed to be equal to the velocity induced by blockage at the corresponding point on the tunnel axis due to the presence of a semi-infinite Rankine body of the same diameter as the model and with the upstream extremity in the same position (for numerical values see appendix). The blockage correction was in no case as large as 5% of the velocity head. The same blockage corrections were applied when the model had a non-zero angle of incidence as in flow with axial symmetry. It is difficult to assess the error due to the various assumptions and approximations made in estimating the blockage: since the estimated correction is relatively small it is reasonable to assume that the error in C_p due to these approximations will never exceed 0.01.

4.4 No correction has been made for pressure changes due to the presence of the support strut. Judging from the results quoted in Ref. 2, the support interference may be expected to cause an error in C_p of about 1% of the velocity head at the rear-most hole in the model and of $\frac{1}{2}$% or less in the important region round the head.

4.5 Taking into account accuracy of measurement, it is believed that the corrected values of C_p given below are accurate to within 1 or 2% of the velocity head.

EXPERIMENTAL RESULTS

5.1 Results are given here for the four head shapes shown in Fig. 4, namely a 2 calibre radius head, ogival head, a 1.5 calibre radius head, ogival head, a 2:1 ellipsoidal head and a 1.732:1 ellipsoidal head.

5.2 The basic measurements for the 2 calibre radius head, ogival head, with the correction for tunnel pressure gradient and blockage already applied, are presented in graphical form in Fig. 5 (a). These measurements are:

(i) pressure distribution along one meridian when the incidence is zero;

(ii) pressure distribution along the meridian, $\theta = 0$, when the incidence has some non-zero value, $5^\circ 44'$ in this case;

(iii) pressure distribution along the meridian, $\theta = \pi$, when the incidence has some non-zero value, $5^\circ 44'$ in this case;

(iv) pressure distribution along the meridian, $\theta = \frac{\pi}{2}$, when the incidence has some non-zero value, $5^\circ 44'$ in this case.

From (i), C_{p_o} is known as a function of the non-dimensional axial distance, $\frac{x}{R}$, from the model nose (where R denotes the radius of the model).

From (i) and (ii) or from (i) and (iii), $\frac{w_1^*}{W}$ can be found as a function of $\frac{x}{R}$: in fact we averaged the values from each and prepared a smoothed curve of $\frac{w_1^*}{W}$ against x/R. From (i) and (iv), w_2^*/W can be found as a function of x/R. Smoothed values of C_{p_o}, w_1^*/W and w_2^*/W are given in the Table: this is all that is necessary for calculating from equation (4) the pressure at any point of the body at any angle of incidence.

5.3 The values of C_p as a function of x along the meridians, $\theta = 0$ and $\theta = \pi$, for the 2 calibre radius head, ogival head at an angle of incidence of $3^\circ 11'$ have been calculated from the data in the Table and are plotted in Fig. 5 (b): measured values are given for comparison on the same graph. The values of C_p as a function of the azimuthal angle θ for various values of x at an angle of incidence of $5^\circ 44'$ have also been calculated from the data in the Table and representative examples are plotted in Fig. 5 (c): measured values are given for comparison on the same graph.

5.4 The corresponding graphs for the $1\frac{1}{2}$ calibre radius head ogival head are given in Figs. 6 (a), 6 (b) and 6 (c); for the 2:1 ellipsoidal head in Figs. 7 (a), 7 (b) and 7 (c); and for the 1.732:1 ellipsoidal head in Figs. 8 (a), 8 (b) and (c). The angles of incidence may appear somewhat curious: the experimental arrangement did not admit of smooth, accurate setting to a predetermined value for the incidence.

5.5 In the transverse flow past a pointed head the foremost point is, of course, a singularity of the potential flow and the considerations of paras 2.1 to 2.8 do not apply in this neighbourhood. Nevertheless for the 2 calibre radius head and 1.5 calibre radius head, ogival noses equation (4) appears from Figs 5 (b), 5 (c), 6 (b) and 6 (c) to be applicable quite close to the point and is certainly equal to the task of determining the magnitude of the suction peak when the angle of incidence takes any value of practical interest (up to 6°, say).

5.6 As x increases along the cylindrical portion of the body, w_2^*/W ought to tend to 2.0 (cf. the two-dimensional flow round a circle). This is realised only roughly in the Table. Interference effects from the support strut may be the cause of the deviation. Also C_p is rather insensitive to the values of w_1^*/W and w_2^*/W; this makes accurate determinations of w_1^*/W and w_2^*/W difficult but it also implies that these parameters do not have to be known very accurately in order to interpolate for C_p with adequate accuracy. For the four head shapes considered, it should be possible, from equation (4) and the data given in the Table, to determine C_p, at any point on the body (apart from the limitations of para. 5.5) at any angle of incidence up to 6°, to within 1 or 2% of the velocity head.

SUMMARY

6. Elementary theoretical considerations have provided a simple picture of the flow over the forward part of a body of revolution in oblique flow. In particular the pressure at any point on the body at any angle of incidence is seen to depend on three parameters which vary along the body. These parameters have been determined by water tunnel measurements for four axially symmetric head shapes. The measurements have been used to illustrate the theoretical conclusions. The data given for each head shape are adequate for a determination of the pressure coefficient at any point on the body at any angle of incidence (up to 6°, say). In particular they can be used to determine the peak suction at any angle of incidence and so the conditions for the onset of nose cavitation.

REFERENCES

1. I. Lotz "Calculation of Potential Flow past Airship Bodies in Yaw". NACA TM 675 (1932).
2. W. B. Huston "Accuracy of Airspeed Measurements and Flight Calibration Procedure". NACA Report 919 (1948).

APPENDIX

BLOCKAGE CORRECTION

The following data used in correcting the experimental results of the present paper, have been taken from some unpublished work by Dr. F. Vandrey.

The velocity in the axis of a closed circular tunnel of radius a at a point at distance x from a source of strength Q on the axis of the tunnel is given by

$$\Delta n = \frac{Q}{2\pi h^2} \left\{ f\left(\frac{x}{a}\right) + \frac{1}{2} \right\}$$

where $f(-x) = -f(x)$. Values of $f(x)$ are given in the following table.

x	f(x)	x	f(x)
0.0	0.000	0.7	0.250
0.1	0.040	0.8	0.276
0.2	0.080	0.9	0.300
0.3	0.119	1.0	0.322
0.4	0.155	1.1	0.342
0.5	0.190	1.2	0.359
0.6	0.218	1.3	0.374

TABLE

2 C.R.H. Ogive				1.5 C.R.H. Ogive			
$\frac{x}{R}$	C_{p_o}	$\frac{w_1}{W}$*	$\frac{w_2}{W}$*	$\frac{x}{R}$	C_{p_o}	$\frac{w_1}{W}$*	$\frac{w_2}{W}$*
0.646	0.237	0.86	2.0	0.149	0.357	0.83	1.7
1.146	-0.045	0.67	1.9	0.298	-0.016	0.64	1.9
1.646	-0.218	0.45	1.9	0.447	-0.255	0.48	2.1
2.146	-0.304	0.27	1.8	0.596	-0.358	0.33	2.1
2.646	-0.213	0.15	1.9	0.745	-0.259	0.23	2.1
3.146	-0.080	0.09	2.0	1.245	-0.098	0.11	2.0
3.646	-0.049	0.06	2.0	1.745	-0.061	0.07	2.1
4.146	-0.032	0.05	2.1	2.245	-0.044	0.05	2.1
4.646	-0.023	0.04	2.2	2.745	-0.034	0.04	2.1
6.646	-0.005	0.03	2.2	4.745	-0.013	0.02	2.1

2:1 Ellipsoid				1.732:1 Ellipsoid			
$\frac{x}{R}$	C_{p_o}	$\frac{w_1}{W}$*	$\frac{w_2}{W}$*	$\frac{x}{R}$	C_{p_o}	$\frac{w_1}{W}$*	$\frac{w_2}{W}$*
0.500	-0.058	0.91	1.6	0.433	-0.016	1.03	1.6
1.000	-0.278	0.58	1.8	0.866	-0.314	0.62	1.8
1.500	-0.330	0.32	1.9	1.299	-0.382	0.37	2.0
2.000	-0.220	0.17	2.0	1.732	-0.286	0.21	2.0
2.500	-0.090	0.10	2.0	2.232	-0.099	0.13	2.0
3.000	-0.051	0.06	2.1	2.732	-0.058	0.08	2.1
3.500	-0.035	0.04	2.1	3.232	-0.040	0.06	2.1
4.000	-0.030	0.04	2.1	3.732	-0.030	0.04	2.1
6.000	-0.010	0.03	2.2	5.732	-0.012	0.03	2.1

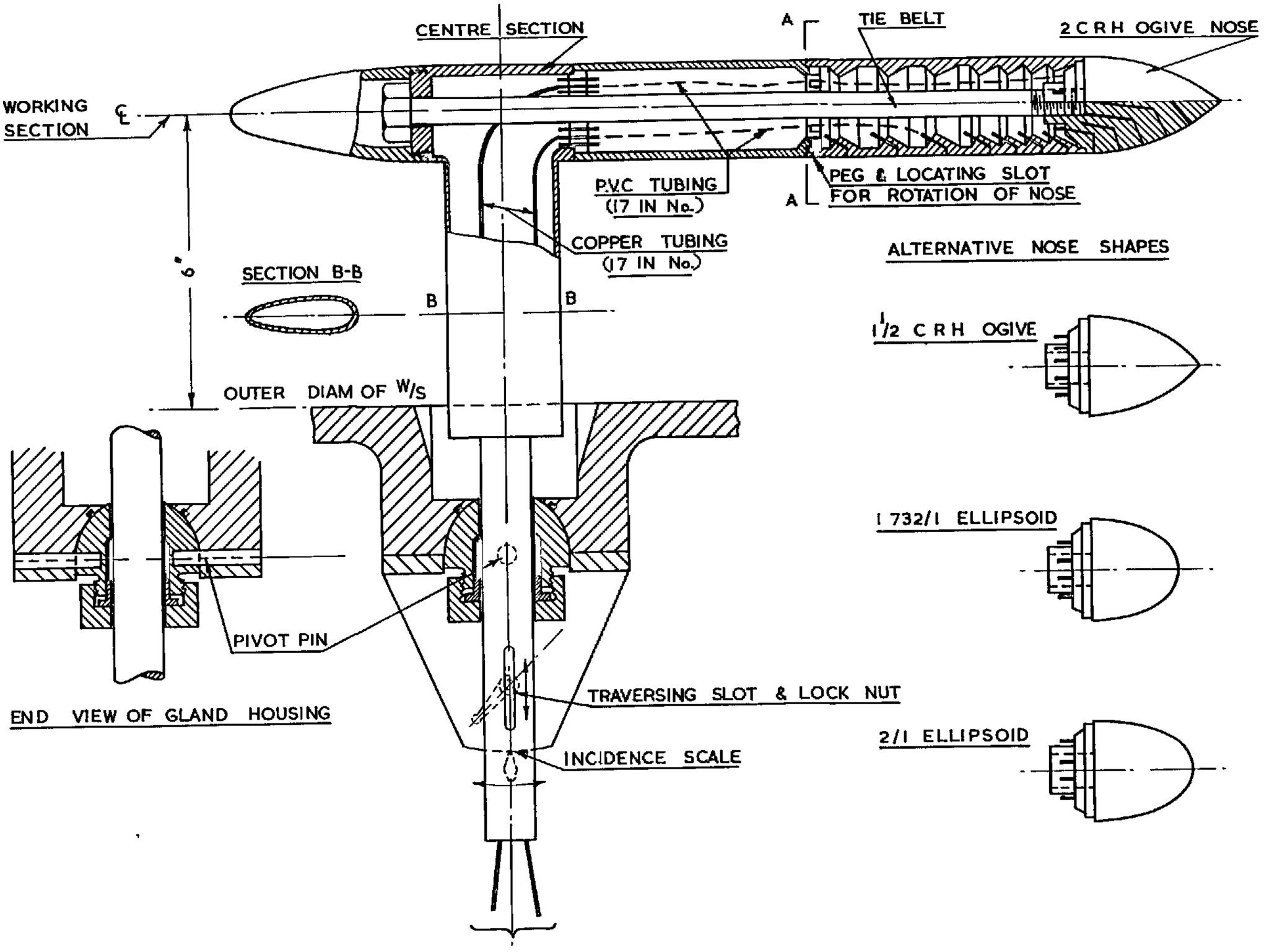

2" DIAMETER PRESSURE PLOTTING MODEL
PART SECTIONED VIEW OF LAYOUT

SCALE APPROX ½ FULL SIZE

FIG.4.

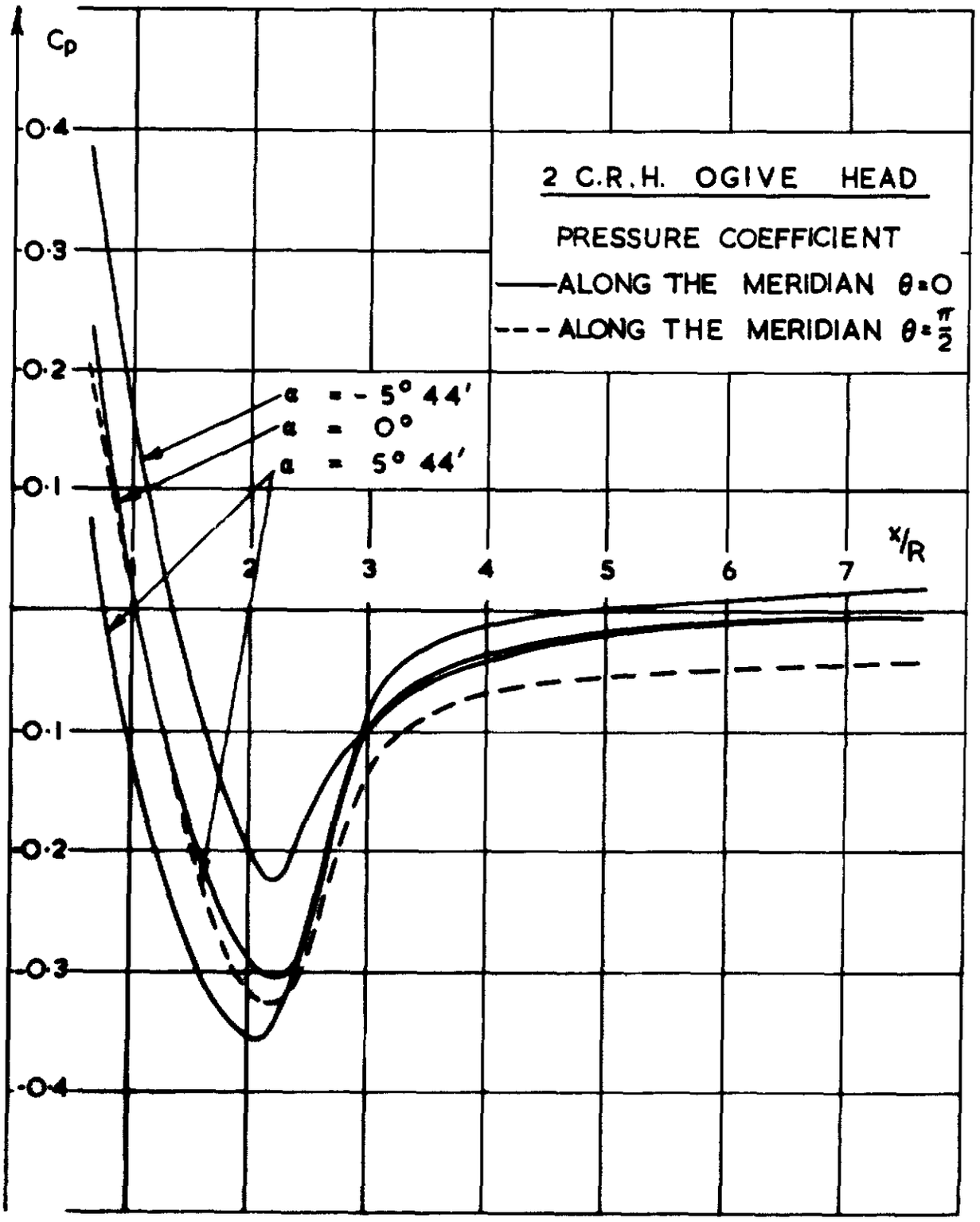
Cp
0·4
0·3
0·2
0·1
0·1
0·2
0·3
0·4
2 C.R.H. OGIVE HEAD
PRESSURE COEFFICIENT
——ALONG THE MERIDIAN θ=0
- - - ALONG THE MERIDIAN θ=π/2
α = - 5° 44'
α = 0°
α = 5° 44'
2
3
4
5
6
7
x/R

FIG.5(a)

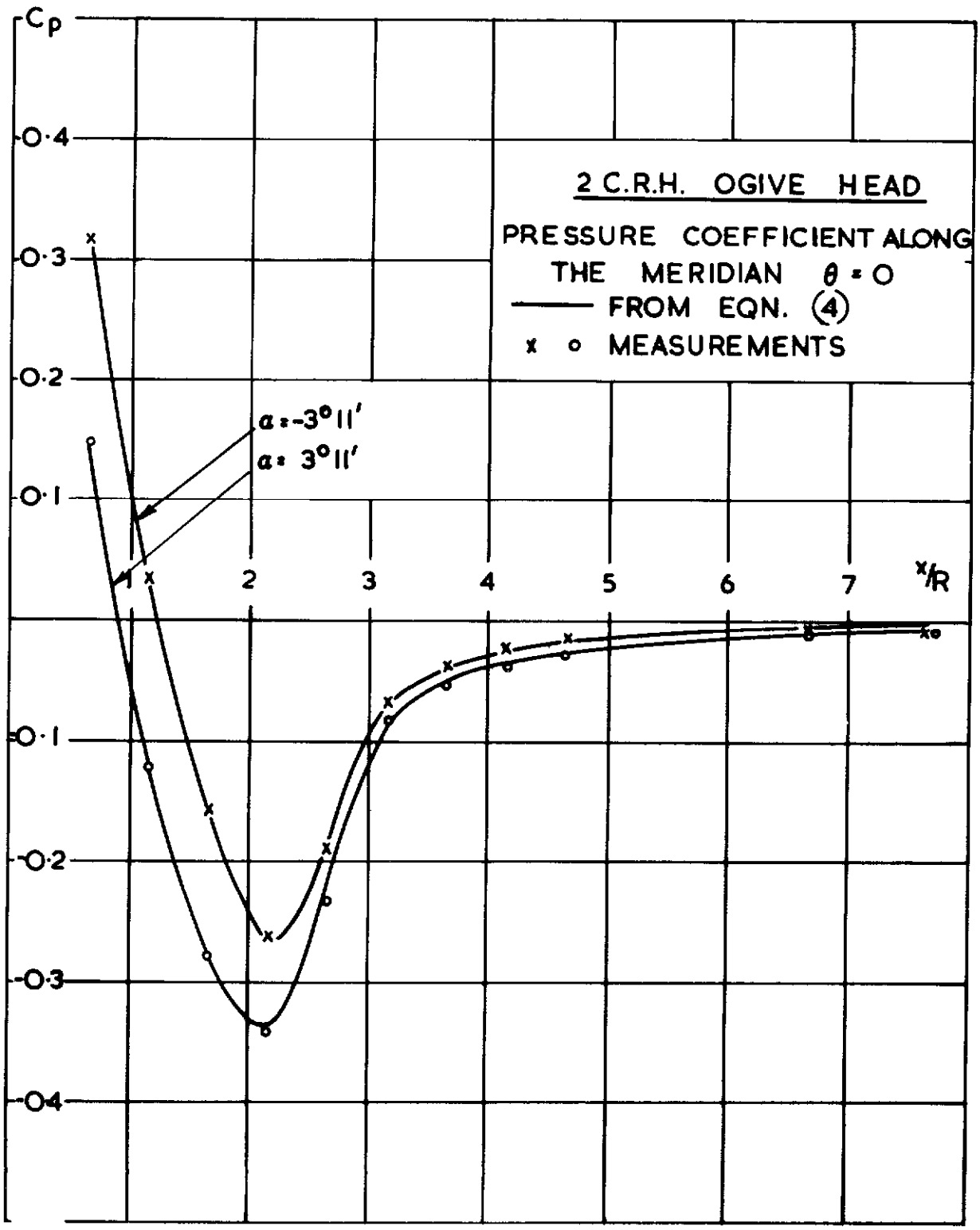
Cp
0·4
0·3
0·2
0·1
2 C.R.H. OGIVE HEAD
PRESSURE COEFFICIENT ALONG
THE MERIDIAN θ = 0
FROM EQN. (4)
x o MEASUREMENTS
α = -3° 11'
α = 3° 11'
1
2
3
4
5
6
7
x/R
0·1
0·2
0·3
0·4

FIG. 5(b)

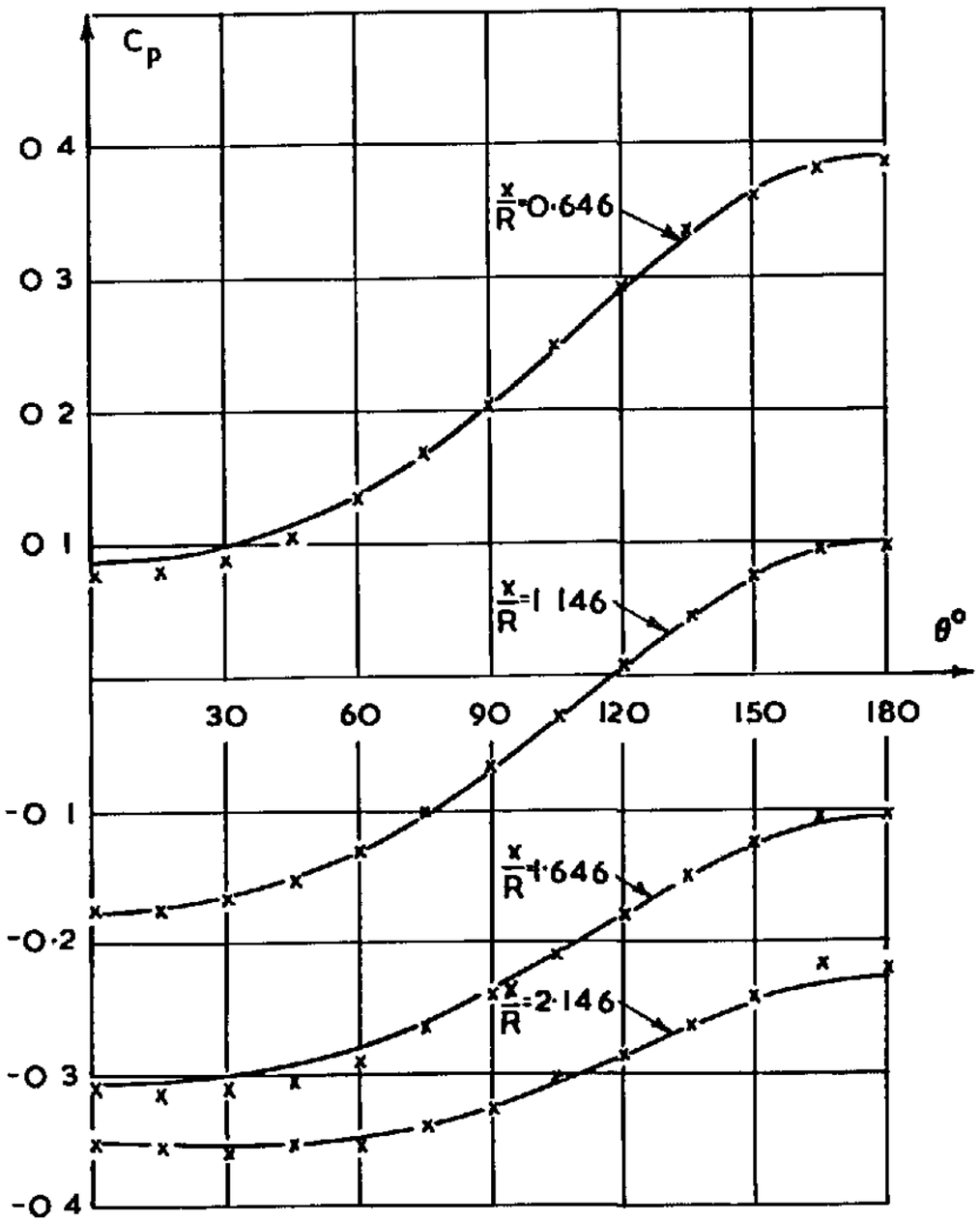

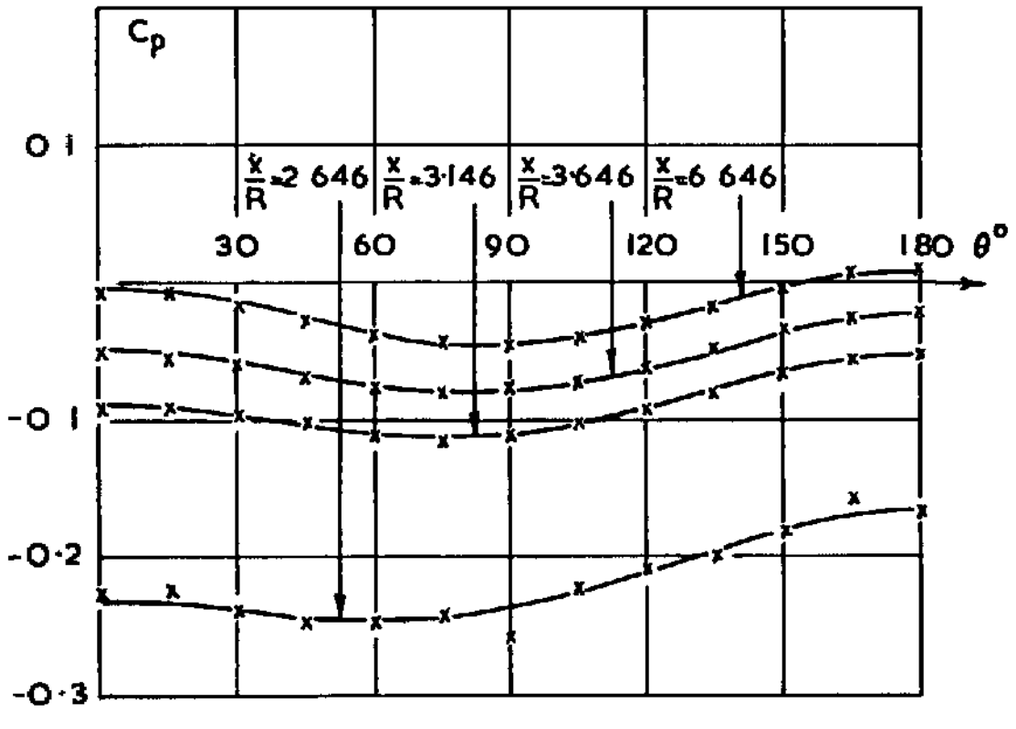

2 C R H OGIVE HEAD

PRESSURE COEFFICIENT AT $\alpha = 5°44'$

—— FROM EQN (4)

x MEASUREMENTS

FIG. 5(c)

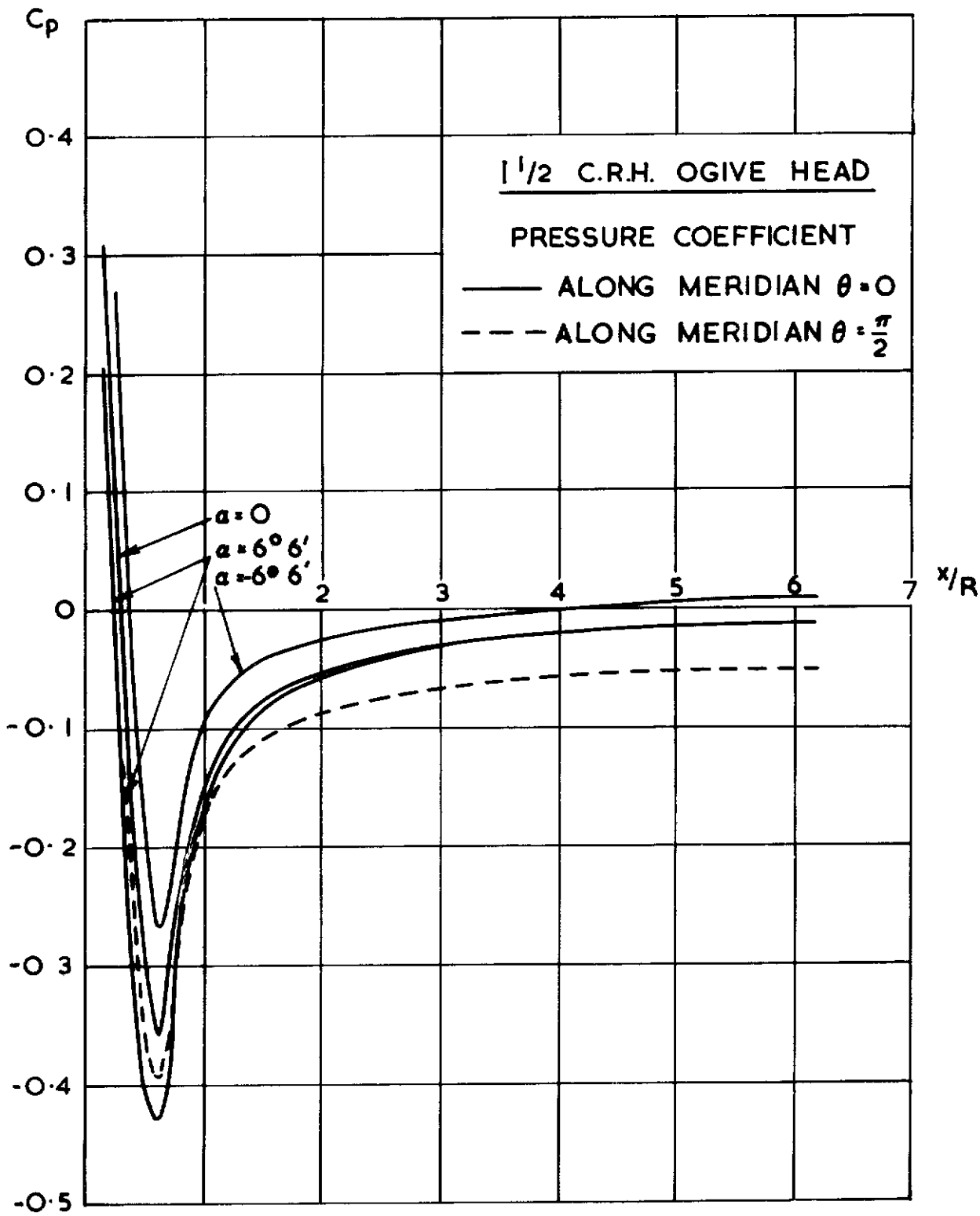
Cp
0·4
0·3
0·2
0·1
0
-0·1
-0·2
-0 3
-0·4
-0·5
1 1/2 C.R.H. OGIVE HEAD
PRESSURE COEFFICIENT
ALONG MERIDIAN θ = 0
ALONG MERIDIAN θ = π/2
α = 0
α = 6° 6'
α = -6° 6'
2
3
4
5
6
7
x/R

FIG. 6(a)

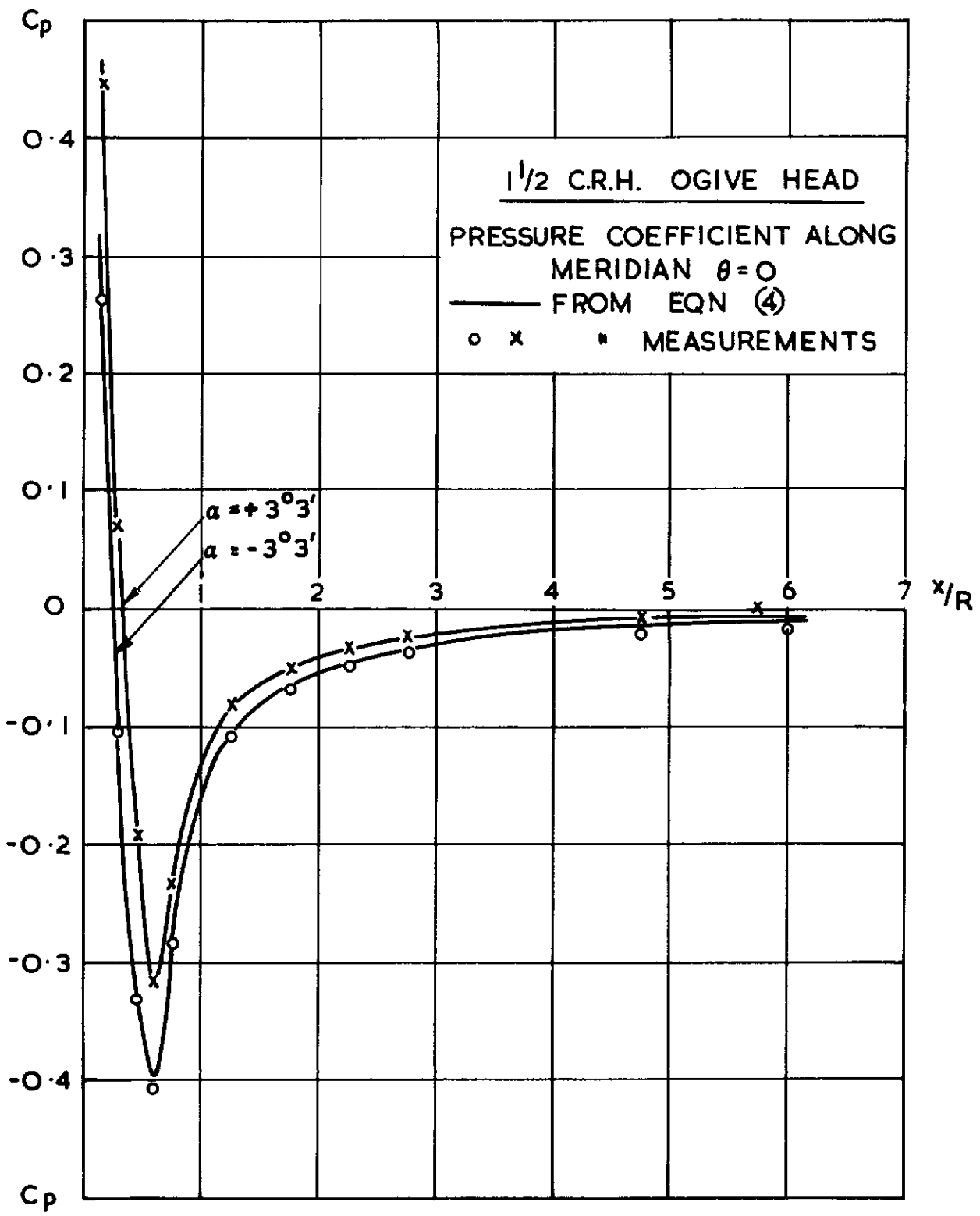
Cp
0·4
0·3
0·2
0·1
0
-0·1
-0·2
-0·3
-0·4
Cp
1 1/2 C.R.H. OGIVE HEAD
PRESSURE COEFFICIENT ALONG MERIDIAN θ = 0
FROM EQN (4)
MEASUREMENTS
α = + 3°3'
α = - 3°3'
1
2
3
4
5
6
7
x/R

FIG. 6 (b)

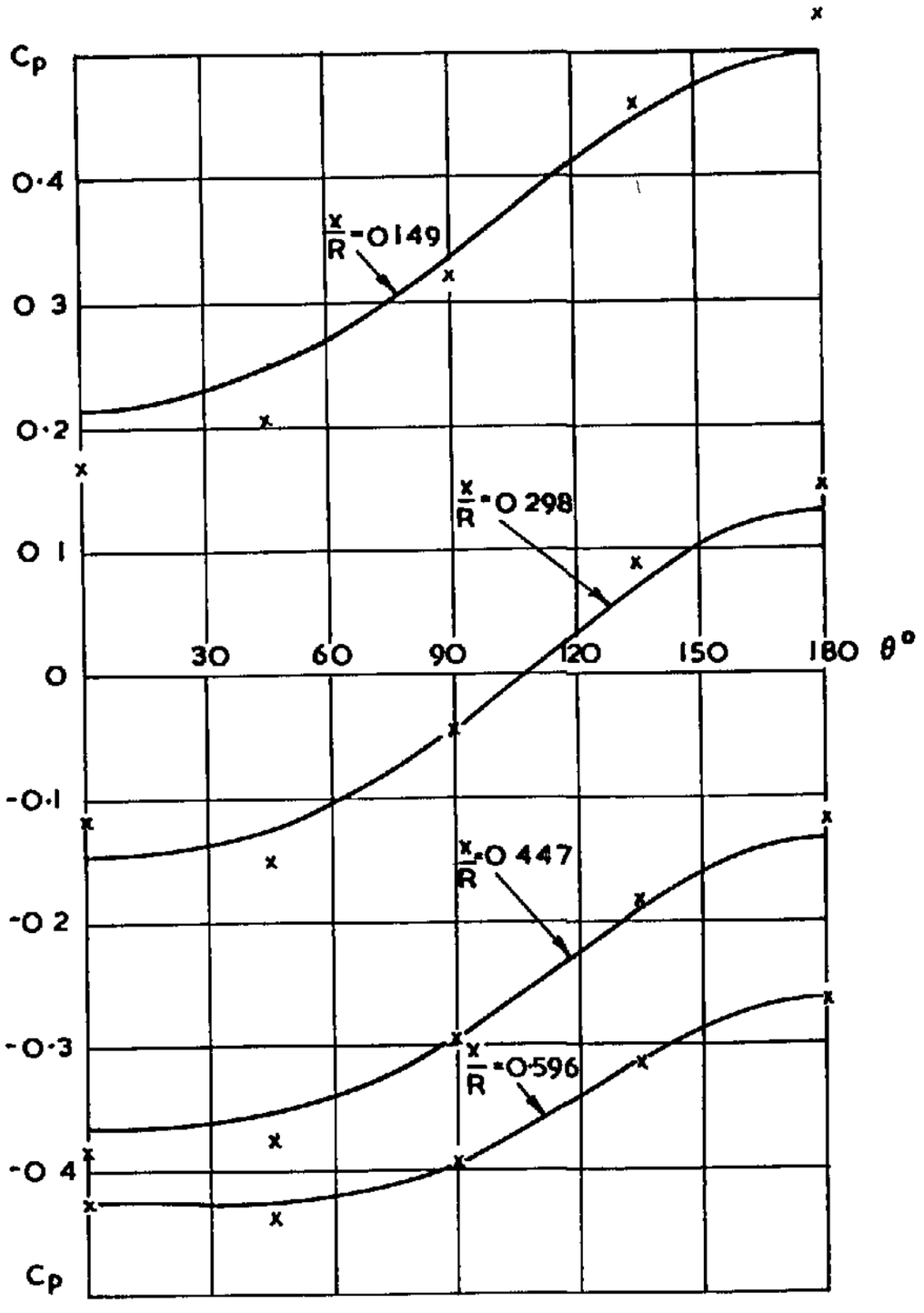
Cp
0·4
0 3
0·2
0 1
0
-0·1
-0 2
-0·3
-0 4
Cp
x/R=0 149
x/R=0 298
x/R=0 447
x/R=0·596
30
60
90
120
150
180 θ°

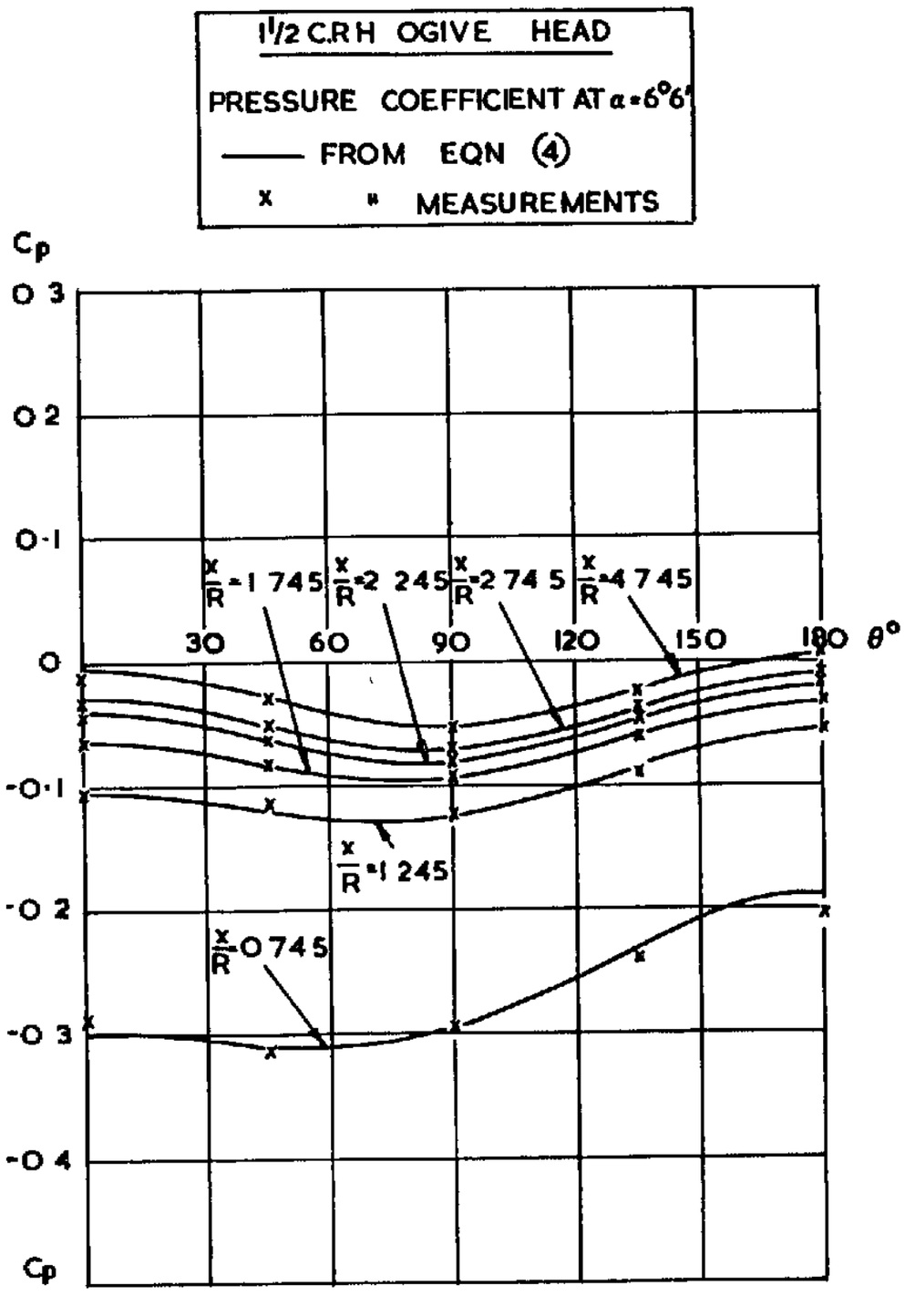
1½ C.R H OGIVE HEAD
PRESSURE COEFFICIENT AT α=6°6'
—— FROM EQN (4)
x " MEASUREMENTS
Cp
0 3
0 2
0·1
0
-0·1
-0 2
-0 3
-0 4
Cp
x/R=1 745
x/R=2 245
x/R=2 74 5
x/R=4 745
x/R=1 245
x/R=0 745
30
60
90
120
150
180 θ°

FIG. 6 (c)

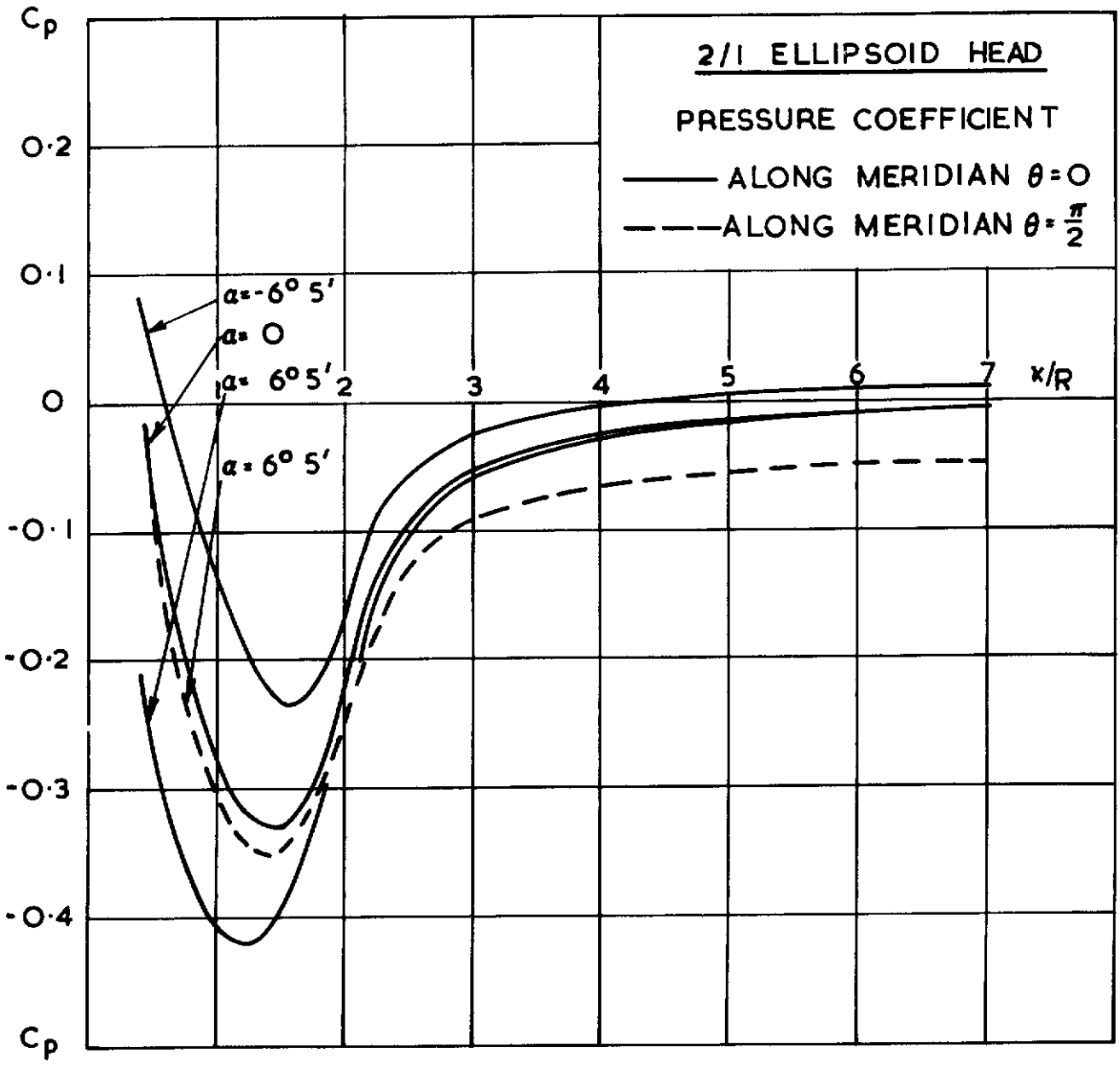
Cp
0·2
0·1
0
-0·1
-0·2
-0·3
-0·4
Cp
2/1 ELLIPSOID HEAD
PRESSURE COEFFICIENT
ALONG MERIDIAN θ=O
ALONG MERIDIAN θ=π/2
α=-6° 5'
α= O
α= 6° 5'
α= 6° 5'
2
3
4
5
6
7
x/R

FIG. 7(a)

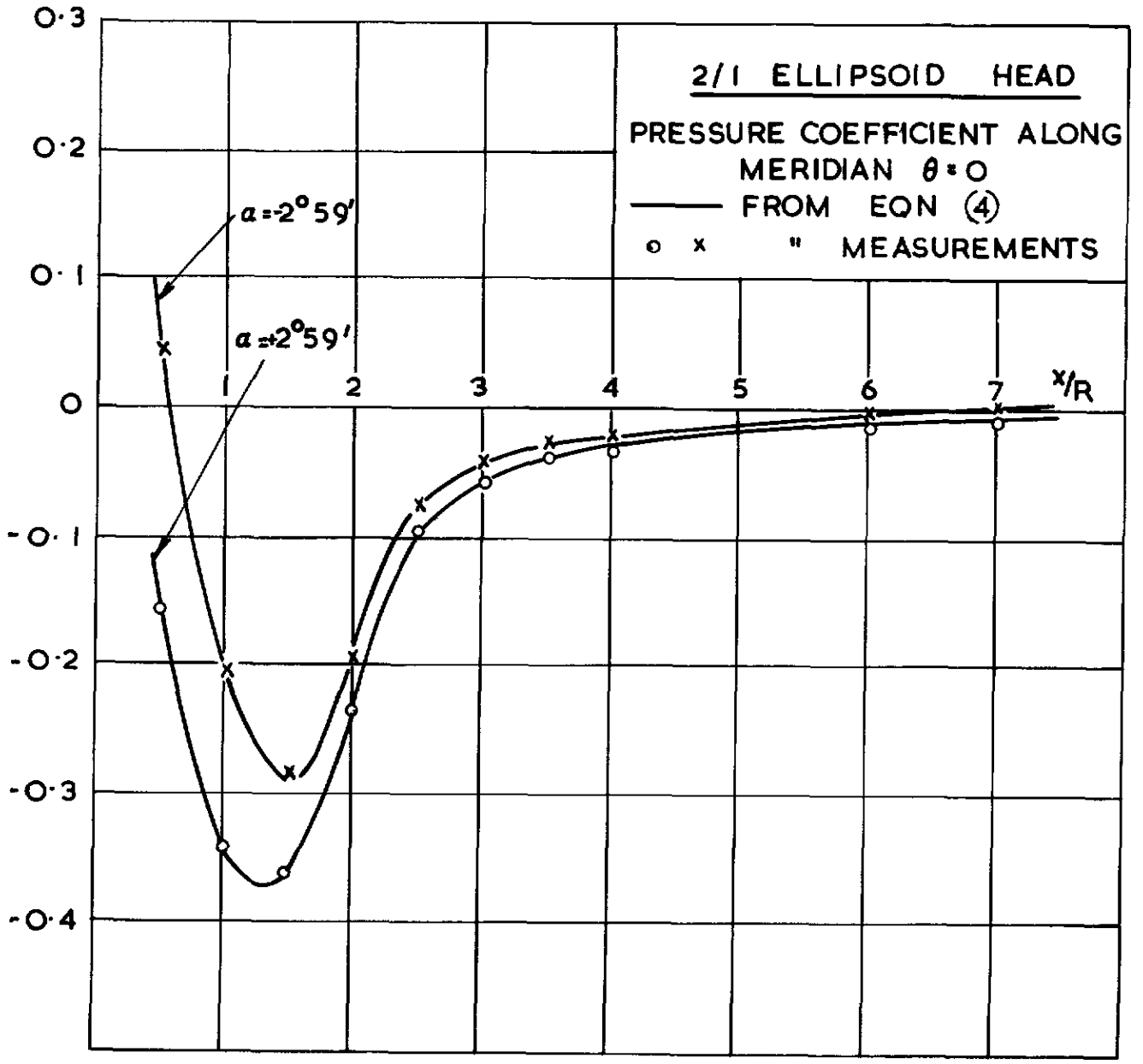
2/1 ELLIPSOID HEAD
PRESSURE COEFFICIENT ALONG MERIDIAN θ = 0
——— FROM EQN (4)
o x " MEASUREMENTS
α = -2°59'
α = +2°59'
0·3
0·2
0·1
0
-0·1
-0·2
-0·3
-0·4
1
2
3
4
5
6
7
x/R

FIG. 7 (b)

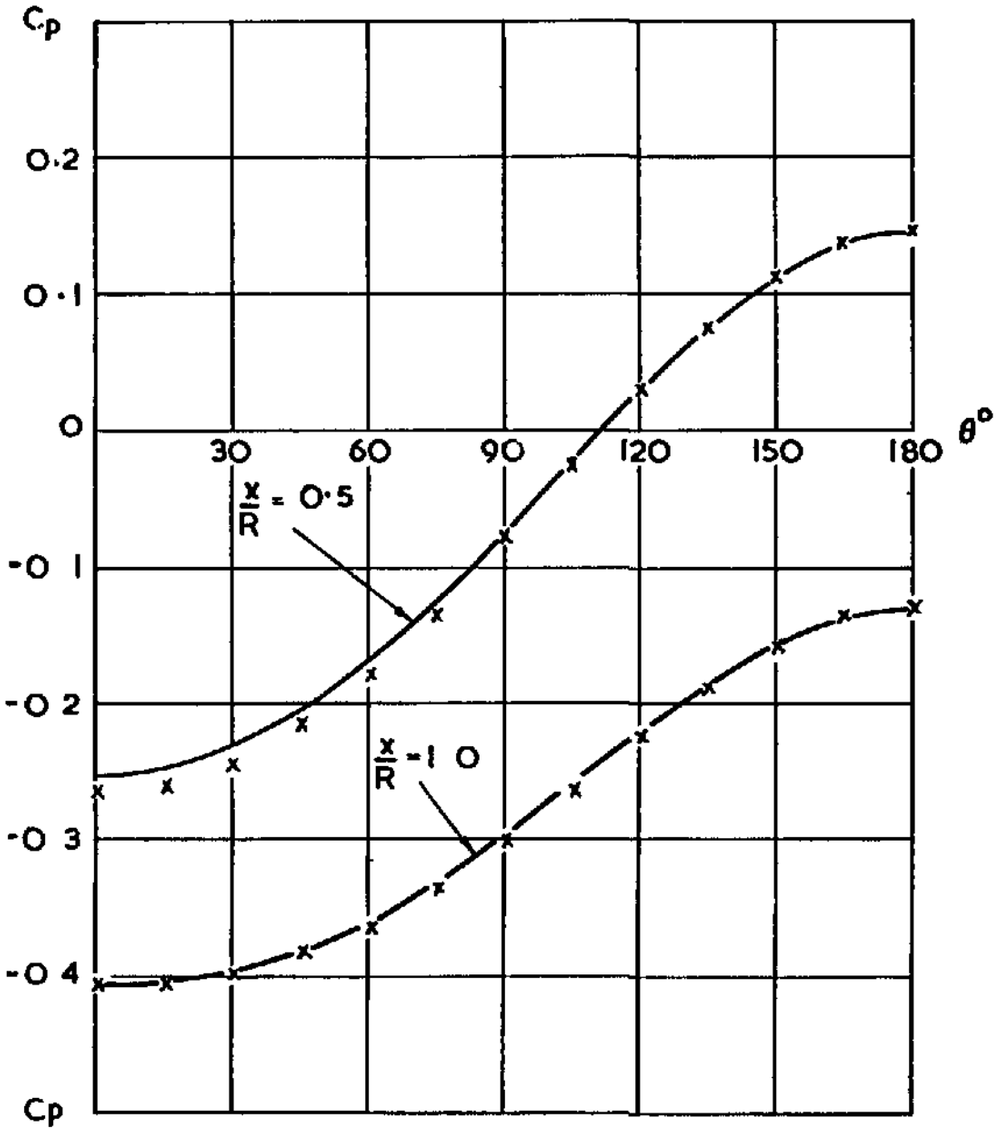

2/1 ELLIPSOID HEAD

PRESSURE COEFFICIENT AT $\alpha \cdot 6^\circ 5'$

—— FROM EQN. (4)

x • MEASUREMENTS

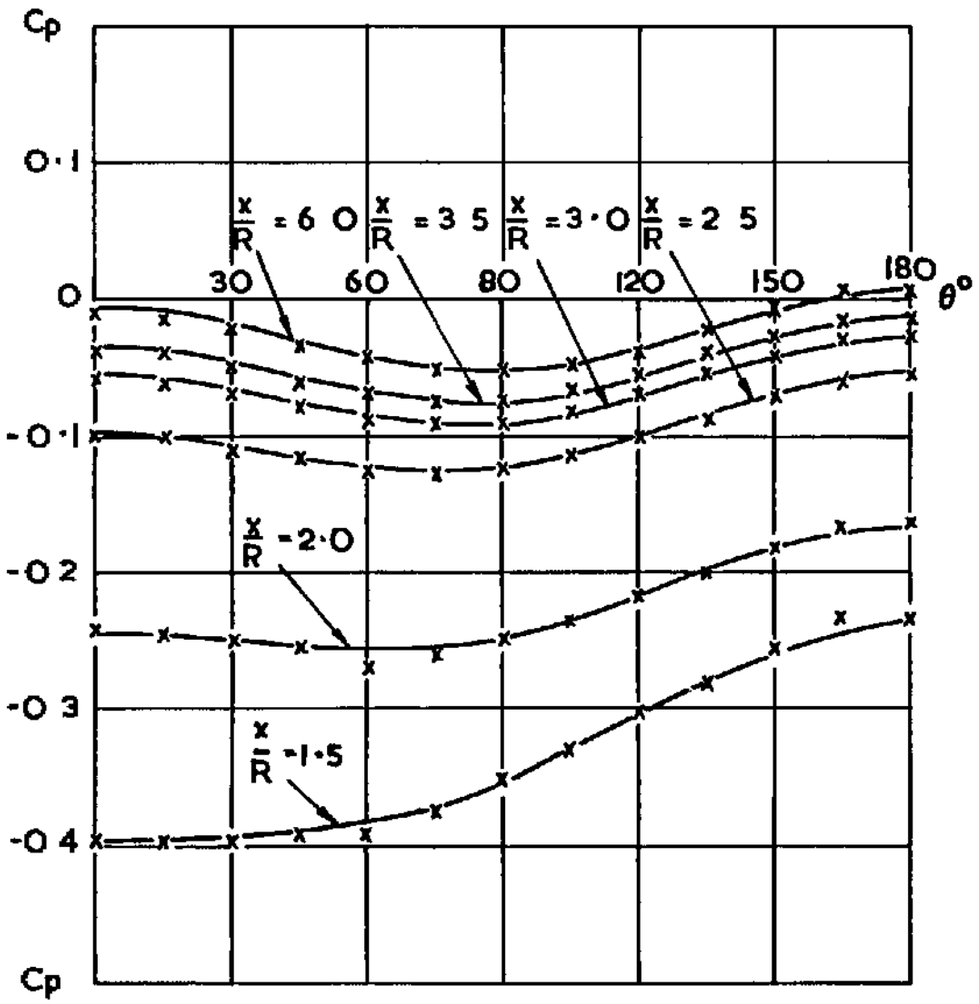

FIG. 7(c)

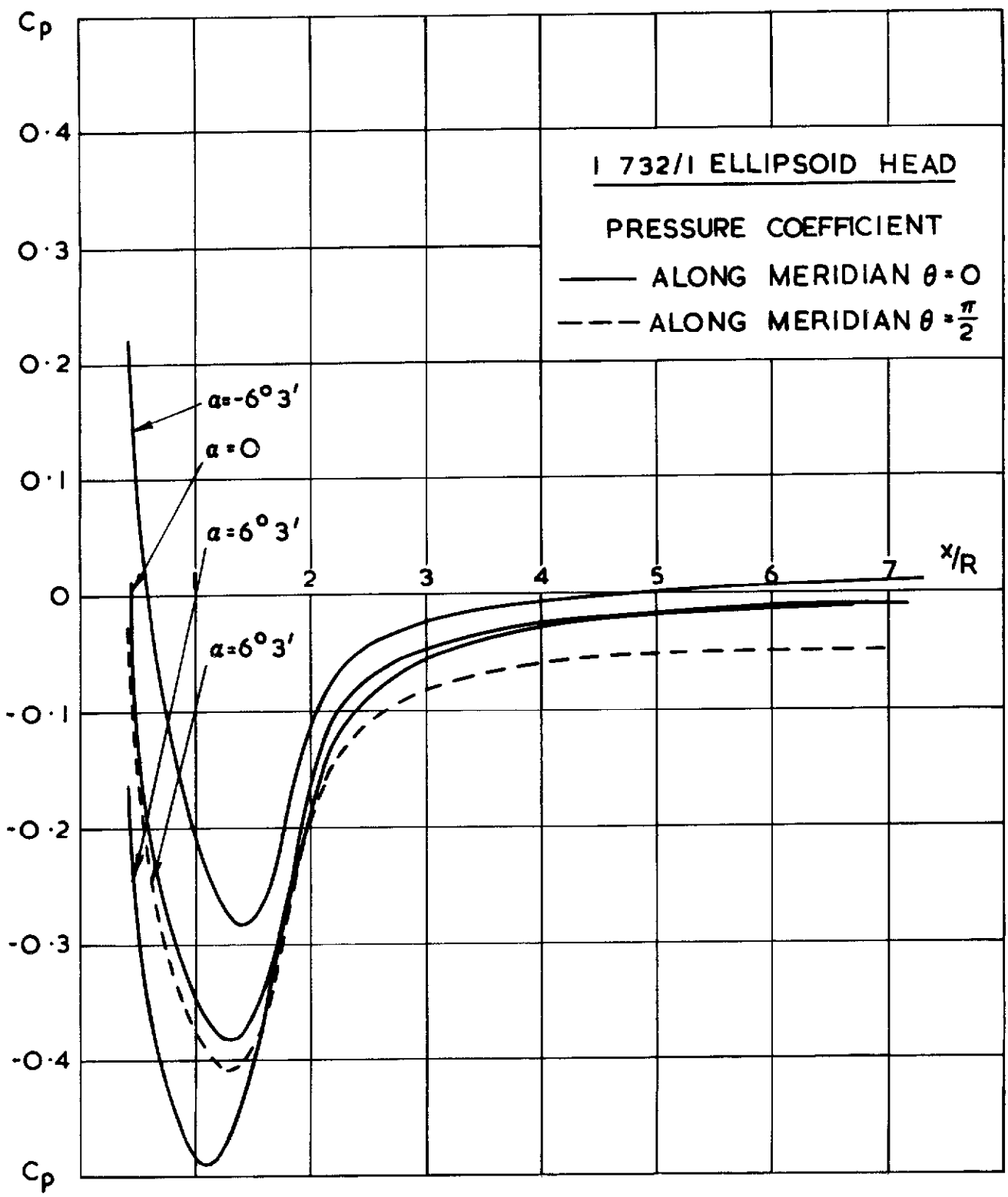
Cp
0·4
0·3
0·2
0·1
0
-0·1
-0·2
-0·3
-0·4
Cp
1 732/1 ELLIPSOID HEAD
PRESSURE COEFFICIENT
ALONG MERIDIAN θ = O
ALONG MERIDIAN θ = π/2
α=-6° 3′
α = O
α=6° 3′
α=6° 3′
2
3
4
5
6
7
x/R

FIG. 8(a)

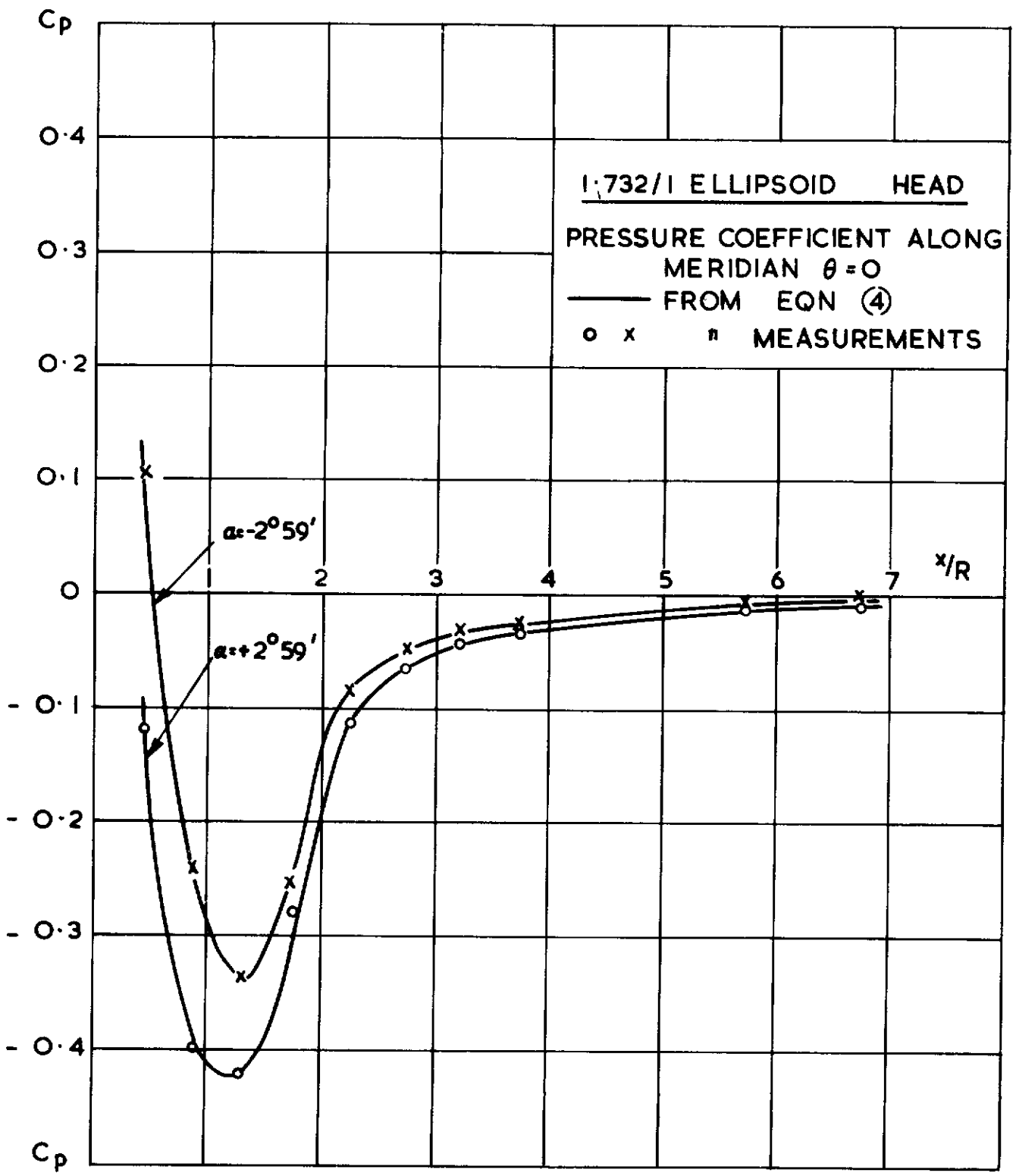
Cp
0·4
0·3
0·2
0·1
0
- 0·1
- 0·2
- 0·3
- 0·4
Cp
1·732/1 ELLIPSOID HEAD
PRESSURE COEFFICIENT ALONG MERIDIAN θ = 0
FROM EQN (4)
o x MEASUREMENTS
α = -2°59'
α = +2°59'
1
2
3
4
5
6
7
x/R

FIG. 8 (b)

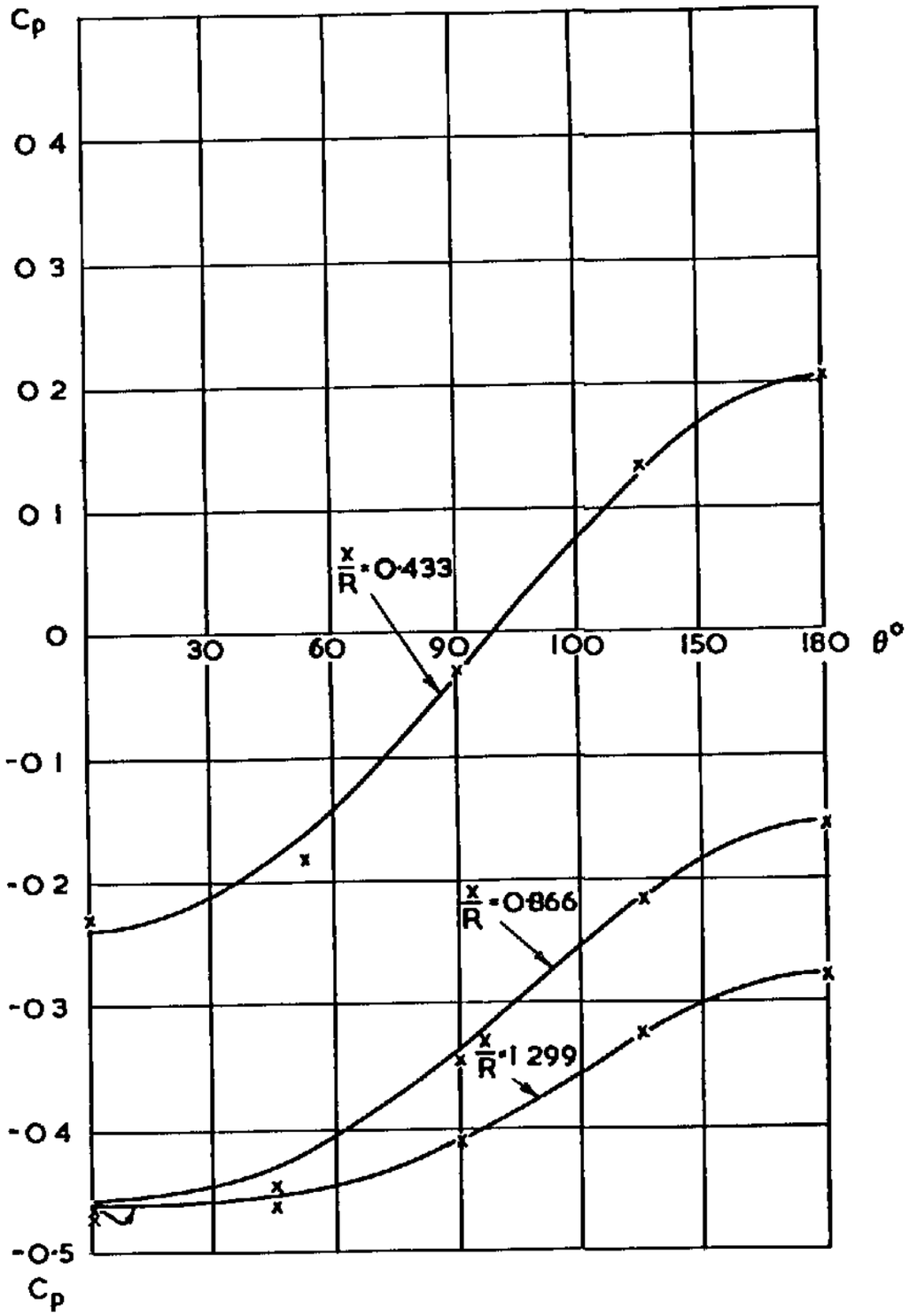

1·732 / 1 ELLIPSOID HEAD

PRESSURE COEFFICIENT AT $\alpha = 6^\circ 3'$

—— FROM EQN (4)

x " MEASUREMENTS

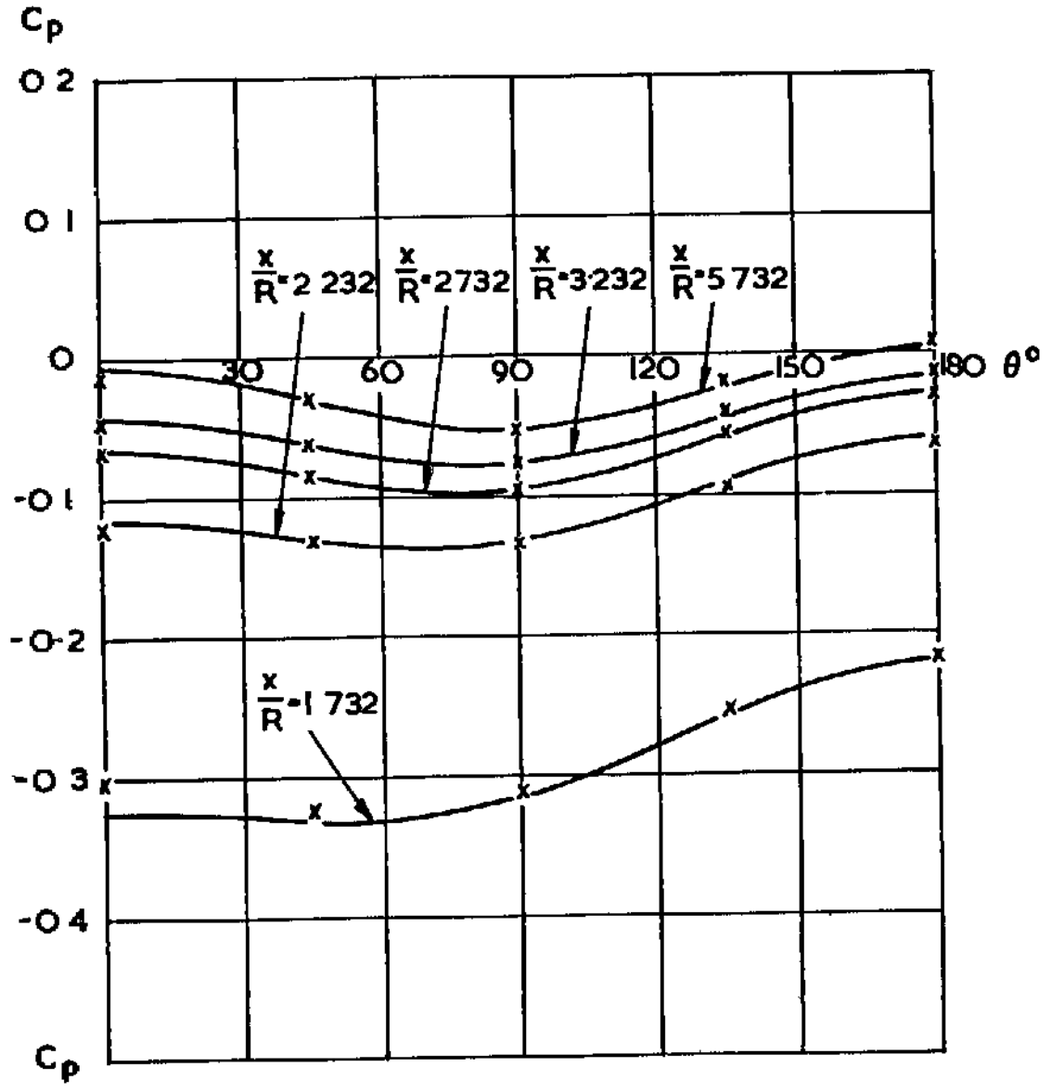

FIG. 8(c)

C.P. No. 213
(16,779)
A.R.C. Technical Report

PRINTED AND PUBLISHED BY HER MAJESTY'S STATIONERY OFFICE

To be purchased from
York House, Kingsway, LONDON, W C 2 — 423 Oxford Street, LONDON, W 1
P O Box 569, LONDON, S E 1
13a Castle Street, EDINBURGH, 2 — 109 St Mary Street, CARDIFF
39 King Street, MANCHESTER, 2 — Tower Lane, BRISTOL, 1
2 Edmund Street, BIRMINGHAM, 3 — 80 Chichester Street, BELFAST
or from any Bookseller

1955

Price 3s 0d net

PRINTED IN GREAT BRITAIN

S.O. Code No 23-9009-13

C.P. No. 213